UNSTEADY BEHAVIOR OF LEADING-EDGE VORTEX AT STATIC AND DYNAMIC MODEL CONDITIONS

Xing Z. Huang
Institute for Aerospace Research/ NRC Canada

Keywords: *unsteady aerodynamics, leading-edge vortex, high angle of attack,*

Abstract

Extensive experimental studies on the unsteady behavior of the leading-edge vortex, especially its breakdown, over delta wings at static and dynamic model conditions were conducted. A 65° delta wing and an 80/65 double delta wing were tested in either roll or pitch at static, periodic (oscillatory or ramp-and-hold motions), and free-to-roll model conditions at free stream velocity up to M=0.3 and Re_{mac} up to $2.4x10^6$. The pitch and roll angles ranged from 0° to 90° at a non-dimensional frequency up to 0.1 and 0.2, in pitch and in roll respectively. Off-surface flow visualization and unsteady pressures at 75% of root chord were measured. Sample results of the 65° delta wing in static and dynamic pitch have been presented and discussed.

Off-surface flow visualization results with the stationary model condition, show that the breakdown region is characterized by an unsteady behavior with axial fluctuations of up to 0.3 C_0, and quite different dissipation rates and propagation speed in breakdown region. While under dynamic model conditions, a deterministic variation in the breakdown location is superimposed. Significant time lags and motion dependence are present both in the movement of vortex breakdown location and in the length of the breakdown region.

The unsteady surface pressures measured at static and dynamic model conditions provide important information about the spectra of the pressure, which indicates the footprint of the vortex. These data further confirm the fluctuations observed in the flow visualizations.

Nomenclature

C_0	root chord	
c_p	pressure coefficient	
f	frequency	
k	thermal conduct coefficient	
m	mass	
M	Mach number	
P	power density	
R	radius	
Re_{mac}	Reynolds number	
St	Strouhal number	$=fx_{VB}/U$
t	time	
T	thermal energy	
U	free stream velocity	
x_{VB}	non-dimensional longitudinal vortex breakdown location	$=X_{VB}/C_0$
X_{VB}	longitudinal vortex breakdown location	
α	angle of attack	
λ	helix rotation frequency of vortex core	
t	convection time	$=C_0/U\cos\alpha$
ρ	density	
ν	dynamic viscosity	
ω	vorticity	
ϖ	non-dimensional frequency	$=\Omega C_0/2U$
Ω	angular rate	

1. Introduction

Highly maneuverabe and agile military air vehicles often have delta-type wings since the formation of leading-edge vortices can generate more lift than straight wings and their compact structure has a weight advantage. A disadvantage, however, is that the leading-edge vortex has unsteady features and may break down under certain conditions. This flow behavior may cause heavy dynamic loads resulting in wing or tail buffeting or cause severe discontinuities in aerodynamic behaviour and loss of controllability.

The unsteadiness of the leading-edge vortex comes from many resources. First when the boundary layer separates from leading edge, the vorticity within the boundary will feed

nonuniformly into the free shear layer. This unsteady filling and other factors lead to the existence of unsteady vortical sub-structures in the free shear layer. Second, as a consequence of an unstable Kelvin-Helmholtz (K-H) instability, the free shear layer, which is under the influence of the vorticity and sub-structure contained in it, rolls up in a spiral fashion and forms a rotational core. Apart from the unsteady K-H instability, steady sub-structures formed by the stationery small-scale vortices also exist in the free shear layer. The sub-structures follow a helical trajectory around the core and the spacing (frequency) causes another source of the unsteadiness. Third, at certain conditions, e.g. at high incidence, the primary vortex core will break down. Downstream from the breakdown point, the core filament abruptly kinks and starts to spiral around at a certain frequency and eventually disintegrates into a "wake-like" turbulent flow. This gives the flow in the vicinity of the spiral a spatial and temporal periodicity that has an effect on the behavior of the pressure distribution on the wing. Finally, there exists a strong axial fluctuation of the vortex breakdown location. As the vortex breakdown has much larger effect on the aerodynamic load and moment than other unsteady aerodynamic behavior, the above axial and related spiral fluctuation (the third and fourth unsteadiness) may have serious impact on the controllability, which leads to the present experimental study.

2. Experimental Set-up

The experiments were conducted at IAR 2m x 3m wind tunnel and at WL's 7 ft x 10 ft SARL facility [1]. The turbulence intensity levels are 0.1% and 0.15% in the IAR and WL tunnel respectively. A 65° delta wing (Fig. 1) and an 80/65° double delta wing models were installed in either rig rolling rig or pitch rig (Fig. 2 and Fig. 3). The roll rig is capable of operating in the forced motion or free-to-roll mode around its body axis. The maximum amplitude for harmonic oscillation is 40° about a maximum roll angle offset ±50° at frequencies up to 18 Hz corresponding to non-dimensional frequency ϖ=0.2 at free stream speed of 100m/sec. The pitch rig could pitch the model around an axis 5.39in downstream of the trailing edge of the delta wing corresponding to 0.33 m.a.c.. The maximum stroke range of angle of attack is from –4° to 93° with minimum transition time of 75 ms resulting in the designed maximum angular rate and angular acceleration are 1900°/s and 79,000°/s^2 respectively.

Tests were conducted at free stream velocities up to M=0.3 and Reynolds number of Re_{mac}= 2.4x10^6. The motions employed were either in roll or pitch planes at static, periodic (oscillatory or ramp-and-hold motions), and free-to-roll model conditions. The range of the pitch and roll angle is from 0° to 90° at the non-dimensional frequency up to 0.1 and 0.2 in pitch and in roll respectively.

The unsteady pressure during static or dynamic model conditions was measured by seven unsteady pressure transducers (Kulite LQ-47-25A) located at x=0.75 of root chord at s=0.92, 0.84, 0.76, 0.68, 0.60, 0.52, 0.44 local semi-span. The maximum sample rates for taking pressure signal were 1k/sec and 0.2k/sec for dynamic and static test respectively. In dynamic model conditions all those data were correlated with the instantaneous motion variables of the model. The very low transducer sensitivity to model acceleration was corrected by means of tare measurement. The static calibration was conducted at beginning of tunnel entry and offset measurement was conducted every 30 minutes. No significant temperature effects were found in the experiments.

The off-surface flow was visualized by seeding the flow with smoke or natural condensation and applying a laser light sheet such that it either located normal to the body axis or longitudinally passed through the vortex core over most of its length. During smoke test the plume of smoke impinges near the nodal point of attachment on windward side so that the smoke goes around the attachment lines and spreads toward the leading edges where it separated. Images were captured by a high-

speed video camera with a frame rate of up to 1000 frames per second.

3. Off-Surface Flow Visualization

Off-surface flow visualization results at stationary model condition exhibit that the breakdown region has significant axial fluctuation. The area of the fluctuation could cover a large portion of the lifting surface.

Examples corresponding to $\alpha = 26°$ are shown in Fig. 4. The vortex filament kink associated with the onset of breakdown is denoted as point A. Aft of this point the axial velocity decreases due to the negative azimuthal vorticity while the circulation continues to grow resulting in an increasing helix angle as well as diameter and eventual breakdown into large scale turbulence (Point B). As can be observed, there is a considerable difference in the appearance of the breakdown region in the these figures. The breakdown region in Fig. 4b is exhibits the slowest dissipation while Fig. 4c shows the fastest. The length in Fig. 4b is nearly 0.3 c_0 which is almost twice that in Fig. 4a and five times that in Fig. 4c, suggesting a high level of unsteadiness and variations in dissipation.

The unsteady responses of points A and B are quite different as shown by the sequence of frames in Fig. 5 for $\alpha = 26°$. It is interesting to see that in the sequence, point A moves in excess of $0.2c_0$ while point B remains more or less stationary. The speed of response of point A can be appreciated in the consecutive pairs. Here the first and second pairs are separated by 0.6 convection times $\tau=c_0/(U_\infty\cos\alpha)$ while the third pair is 0.15τ apart. These pairs show the approximate maximum observed speed of propagation of point A which corresponds to $0.5U_\infty\cos\alpha$ whereas point B barely moves at all. In addition, when point A is close to point B the helix angle is smaller and the pitch of the spiral core remains more or less constant.

Images exhibiting several clear helix loops were thus used to determine the local non-dimensional helical wavelength and the Strouhal number of the spiral rotation of the vortex core as shown in Fig. 6 together with data from others' measurements [2], [3], where the Strouhal number of the spiral rotation is defined as:

$$St = \frac{fx_{VB}}{U_\infty} = \frac{\cos\alpha}{\bar{\lambda}} \qquad (1)$$

and f is the rotation frequency of the helix. St number varies within the range of 4 ~ 14 over the tested range of angles of attack.

Under dynamic model condition a deterministic variation in the breakdown location is superimposed to the previously discussed unsteady behavior. Significant time lags are present in the position of the instantaneous locations of point A and B with respect to their corresponding average static locations. Fig. 7 shows examples of the motion histories in pitch-up or pitch-down α: 60° ↔ 0°. While the corresponding movements of point A and B are shown in Fig. 7b and 7c for pitch-up and pitch-down respectively. The averaged static points are superimposed for comparison. In addition to the aforementioned delay in the positions of breakdown, it is clear that during pitch-up the distance between points A and B is larger than under static conditions, reflecting the ability of A to move faster than B, while during pitch-down the distance is dramatically reduced as the former "catches up" with the latter. The random breakdown fluctuations can also be observed in the figure. More images are shown in Fig. 8 as examples. They were taken from pitch-down and two consecutive frames corresponding to a differences of $\Delta\alpha$=-0.03° and separated by 0.15τ. The point A moved upstream by more than $0.1c_0$ as opposed to the expected, albeit small, aft movement during pitch-down motion.

The unsteady pressure measurements shown below will further consolidate the above observations and supply the useful spectra and power density function in different model situations.

4. Unsteady Pressure Measurements

As mentioned before this paper emphasizes on the studying of axial and spiral fluctuation

caused by vortex breakdown. The sample rate in the pressure measurement was chosen to cover that frequency domain only. Thus these unsteady sources, e.g. fluctuation in vorticity feeding, free shear layer and rotation of vortex core, may not be measured. Part of the reason was the difficulties in raising sample rate at high speed and high Re number flow conditions. As the current experiments were conducted at the speed of M≈0.3 and $Re_{mac}=2.4x10^6$, unlike other reported experiments conducted at much lower speed, the sample rate in current experimental study should be at least 4k/sec to obtain reasonable St number (St≈4.5) if the unsteady sources in vorticity feeding and free shear layer to be touched. Moreover owing to limited space, only some results of the 65° delta wing in pitch plan, either in static or dynamic, are presented here. More information about unsteady pressure measured in pitch, roll and free-to-roll conditions can be found in Ref. [4]

The pressure measurements under static model conditions at several typical angles of attack are shown in Fig. 9a to Fig. 9f for different angles of attack, e.g. 1) α=1°; 2) α= 16°; 3) α=25° and 29°; 4) α=47° and 5) α=51°. These angles of attack are corresponding to different flow states: 1) no separation, 2) weakly vortex forming, 3) strong vortex and breakdown across the transducer, 4) strong reverse flow and 5) wake flow.

At α=1° the signals from the pressure transducers shown in Fig. 9a can be taken as the back ground noise from the wind tunnel since there is no flow separation. When angle of attack increases to the second period (α=16°), there are clear peaks that appear at high frequencies and at the pressure transducers P3 to P5 as seen in Fig. 9b, indicating the existence of spiral vortex. Further increasing the angle of attack, results in the vortex breakdown location moving close to the transducers, and a fluctuation in the lower frequency band becomes obvious as illustrated in Fig. 9c to 9d for α=25° and 29° respectively. These figures confirm the existence of a serious axial fluctuation in the vortex breakdown location as observed in flow visualization experiments. When vortex breakdown is near the apex, the spiral and reverse flow remain alive until the flow becomes separated wake flow at even higher angles of attack. The corresponding pressure footprint can be found in Fig. 9e and 9f for α=47° and 51° respectively. At α=47° there are some remarkable pressure fluctuations at f=18Hz, corresponding to St=0.84. While at α=51° this peak moves to a lower frequency, indicating a large-scale low frequency wake-like flow pattern.

Under dynamic conditions much more profound information about the unsteady pressure has been found. As examples, Fig. 10 to Fig. 16 show the unsteady pressure measurements, either in the time domain or in the frequency domain, at pitch-up or pitch-down conditions (α: 50°↔70°, 10°↔70°, 20°↔40° and 30°↔40°).

Fig. 10 and Fig. 11 show the unsteady pressures during pitch-up (α: 50°→70°) or pitch-down (α: 70°→50°) respectively. The time period is 0.675sec. These pressure measurements are the simplest among the other test cases as there is no vortex breakdown and spiral flow involved. The pressures in the time domain show that there is neither a noticeable phase shift between the motion and the measured pressure nor phase shift between pressures obtained in different pressure transducers. The spectra show that there very little power other than that at the primary motion frequency.

Comparing the pressure footprints for the cases when there is a simple vortex, vortex breakdown, or spiral flow appears, is much more complex. Fig. 12 and Fig. 13 show the unsteady pressures at pitch-up (α: 10°→70°) or pitch-down (α: 70°→10°) respectively at Δt=0.675 sec. The results in time domain show that the pressure response functions at each pressure transducer are quite different. Also there are quite significant phase shifts between the different pressure transducers, indicating there exists a spanwise wave in pressure. The spectra shown in Fig. 14 exhibit that, in addition to the primary motion, the axial and spanwise fluctuation of the vortex and its breakdown

location may result in a noticeable power density at higher frequencies.

The above complex spectral and spanwise phase shift become even vigorous when the vortex and its breakdown occupy the major period of the motion. As examples Fig. 14 and Fig. 15 show the unsteady pressure spectra and time histories measured at each pressure transducer for pitch-up (α: 20°→40°) or pitch-down (α: 40°→20°) respectively at Δt=0.675 sec. In the time domain there are almost opposite pressure response functions between pressures at transducers P1 to P3 and P4 to P6, while the pressure response function in P7 takes another shape. These figures clearly demonstrate that the vortex and its breakdown will result in a much stronger spanwise wave compare with to the case no vortex or vortex breakdown.

5. Discussion

As observed the vortex and its breakdown is characterized by many unsteady facts. Since the vortex breakdown region has a significant length compared with the dimensions of aircraft lifting surfaces and the vortex and its breakdown have a dominant effect on the flight mechanics, it necessary to have a good understanding of this flow behavior. The following discussion will first explain the different unsteady behaviors within the vortex breakdown region leading to axial and spanwise fluctuations.

In order to explain the different response characteristics of point A and point B it is helpful to invoke the vorticity transport equation [4]:

$$\frac{D\omega}{Dt} = \omega \cdot \nabla U + \nu \nabla^2 \omega \qquad (2)$$

where the first term on the right represents the change in vorticity due to stretching or turning of the vortex core while the second term is the net rate of viscous diffusion of vorticity. Just downstream of point A the first term is much larger than the second one and the latter can be ignored. Thus at point A Eq. (2) can be written for the x component using the index notation [5]:

$$\frac{D\omega_1}{Dt} = \omega_1 \partial_{(1} u_{1)} + \omega_2 \partial_{(2} u_{1)} + \omega_3 \partial_{(3} u_{1)} \qquad (3)$$

where the first term of the RHS corresponds to the vorticity generated by streching the vortex core, while the second and third terms reflect the vorticity generated by tilting of the core. All three terms are directly affected by axial pressure disturbances [6], [7] resulting in the fast response speed of point A.

At point B, on the other hand, the first term is negligible compared with the second term and Eq. (2) becomes:

$$\frac{D\omega}{Dt} = \nu \nabla^2 \omega \qquad (4)$$

which has the same form as the thermal energy equation for incompressible flow with constant temperature boundaries.

$$\rho c_p \frac{DT}{Dt} = k \nabla^2 T \qquad (5)$$

implying that there is an analogy between vortcity and temperature [8], which suggests that $D\omega/Dt$ is characterized by relatively long time scales that result in the observed slow reaction speed of point B. The circulation of the vortex is gradually destroyed by viscosity after the kink. Smaller core deflections from the intact vortex axis are associated with lower shear stresses, resulting in less vorticity dissipation than those associated with larger deflections. Consequently lower spiral divergence of the core leads to longer breakdown regions, as seen in the experiments.

When point A is close to point B the absolute value of the azimuthal vorticity increases rapidly after the kink leading to a faster spiral divergence, smaller helix angle and thus better defined dark circles corresponding to sections of the tilted vortex core. If the pitch of the spiral core remains more or less constant as observed, it therefore appears that the length of the breakdown region changes mainly as a result of changes in the number of spiral turns contained therein. The additional loops needed to lengthen the breakdown region seem to be

generated by a curling up of the previously intact vortex just forward of point A. Likewise a straightening of the upstream turns within the breakdown region seems to cause its shortening.

The spanwise fluctuation can be explained by momentum conservation for the spiral flow within the vortex breakdown region. For simple purpose, assuming the intact vortex is quasi-cylindrical and made up of an inner viscous core surrounded by an essentially inviscid rotational flow field. Applying angular momentum conservation normal to the local vortex axis at two instants (t_1 and t_2) corresponding to locations just upstream and merely downstream of the vortex kink respectively:

$$\frac{1}{2}mr_c^2\Omega_{c1} = \frac{1}{2}mr_c^2\Omega_{c2} + mr^2\Omega \qquad (6)$$

where m is the mass of the slice , r_c is the radius of the viscous core, Ω_{c1}, Ω_{c2} are the rotation rates of the slice around the local vortex axis at times t_1 and t_2 respectively, and Ω is the angular rate of the deflected slice around the intact vortex axis. Brücker [9] found experimentally that $\Omega \approx \Omega_{c1}/3$ at $r \approx r_c$ which on the basis of the above equation leads to $\Omega_{c2} \approx \Omega_{c1}/3$. Thus the spiral vortex core in the breakdown region will introduce spanwise fluctuation whose frequency may be only one third of the rotational vortex core as measured in pressure transducers.

6. Conclusions

- The leading-edge vortex breakdown region exhibits strongly unsteady characteristics. There exist strong axial and spanwise fluctuations when vortex breakdown involved.
- The vortex breakdown region consists of two quite different states: the onset of vortex breakdown (point A) and the point of breakdown to large scale turbulent (point B).
- Point A appears to have a much faster response to disturbances than point B.
- Under some conditions the slow response of point B limits the motion of point A. The two different response speeds result in significant stretching and compression of the breakdown region.
- Under dynamic conditions the distance between point A and B increases during pitch-up and decreases during pitch-down.
- The Strouhal number of a spiraling vortex core depends on angle of attack and breakdown location.

References

[1] Hanff, E.S. and Huang, X.Z. Wind Tunnel Experiments of Delta and Double Delta Wing Rolling or Pitching at High Rates and High Incidence. Vol. I: General Description and Highlight of Results, IAR LTR 97-013, 1998.

[2] Lambourne, N.C. and Bryer, D.W. The Bursting of Leading-Edge Vortices – Some Observations and Discussion of the Phenomenon. ARC R&M No. 3282, April 1961.

[3] Traub, L.W. etc. Instabilities of Vortex Breakdown: Their Structure and Growth. AIAA Paper 95-0585, 1995..

[4] Huang, X. Comprehensive Experimental Studies on Maneuvering Aerodynamics over Delta Wing Configurations in IAR – Vol. 3. Unsteady Pressure Results. IAR Rep. To be published in 2004.

[5] Batchelor, G.K. *An Introduction to Fluid Dynamics* Cambridge University Press 1967.

[6] Panton, R. *Incompressible Flow* Wiley-Interscience Publication. John Wiley &Sons, 1984.

[7] Darmofal, D.L. The Role of Vorticy Dynamics in Vortex Breakdown, AIAA Paper 93-3036, 1993.

[8] Hall, M. G. *Vortex Breakdown,* Annual Review of Fluid Mechanics, No. 4: 195-218.

[9] Brücker, Ch. Study of Vortex Breakdown by Particle Tracking Velocimetry (PTV). Part 2: Spiral – Type Vortex Breakdown. *Exp. In Fluids*. 14, 1993, pp.133-139

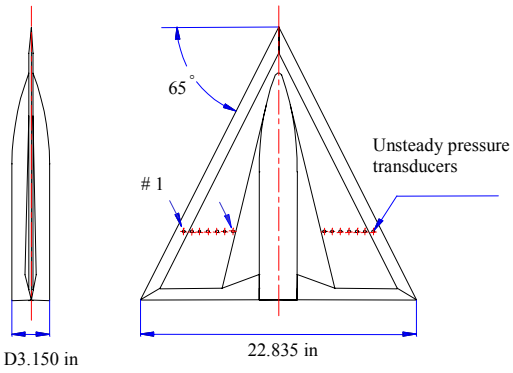

Fig. 1 65° delta wing model

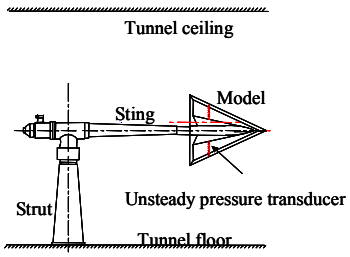

Fig. 2 Roll rig

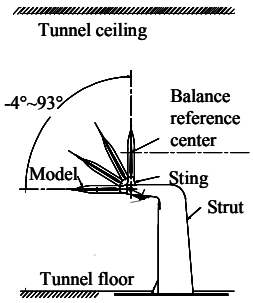

Fig. 3 Pitch rig

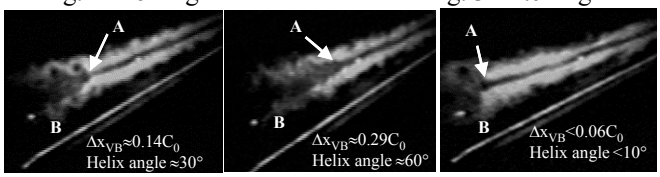

Fig. 4 Different vortex breakdown appearances (σ=26°)

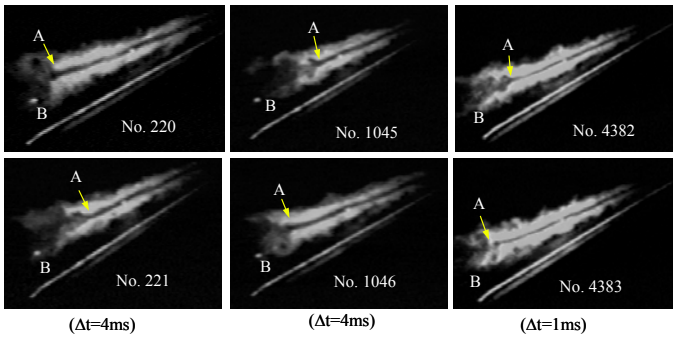

Fig. 5 Image pairs of vortex breakdown appearances

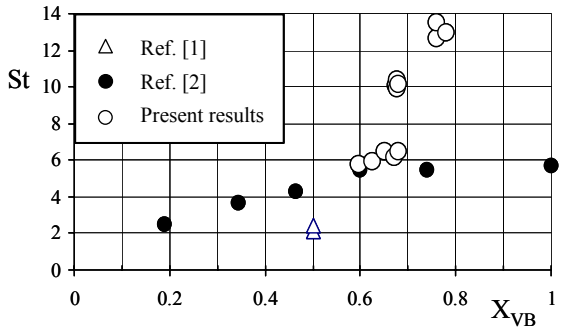

Fig. 6 Strouhal number of spiral breakdown pattern

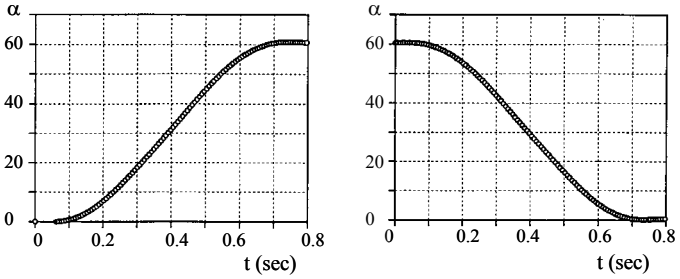

Fig. 7a Pitch-up and pitch-down motion histories

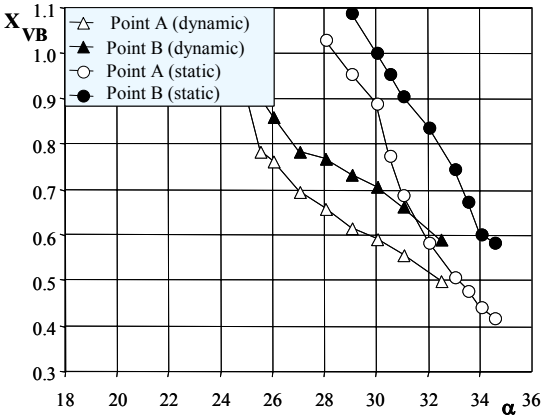

Fig. 7b pitch-up (0°→60°)

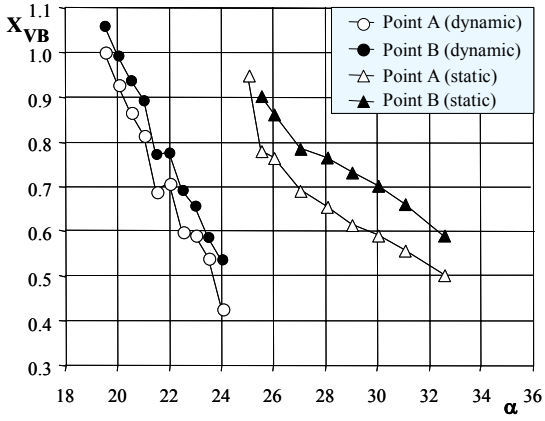

Fig. 7c pitch-down (60°→0°)

Fig. 7 Movements of vortex breakdown location at static and dynamic situations

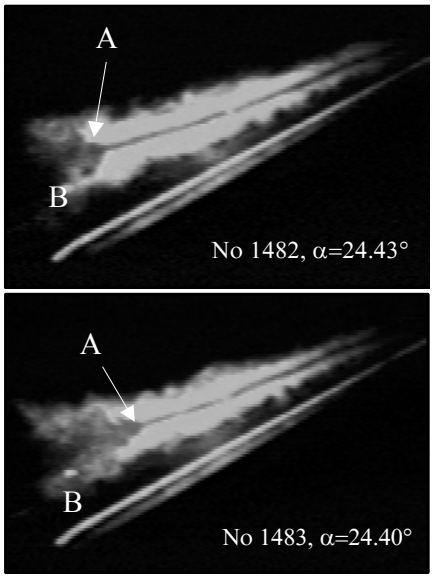

Fig. 8 Breakdown fluctuation during pitch-down motion (α:50°→0°)

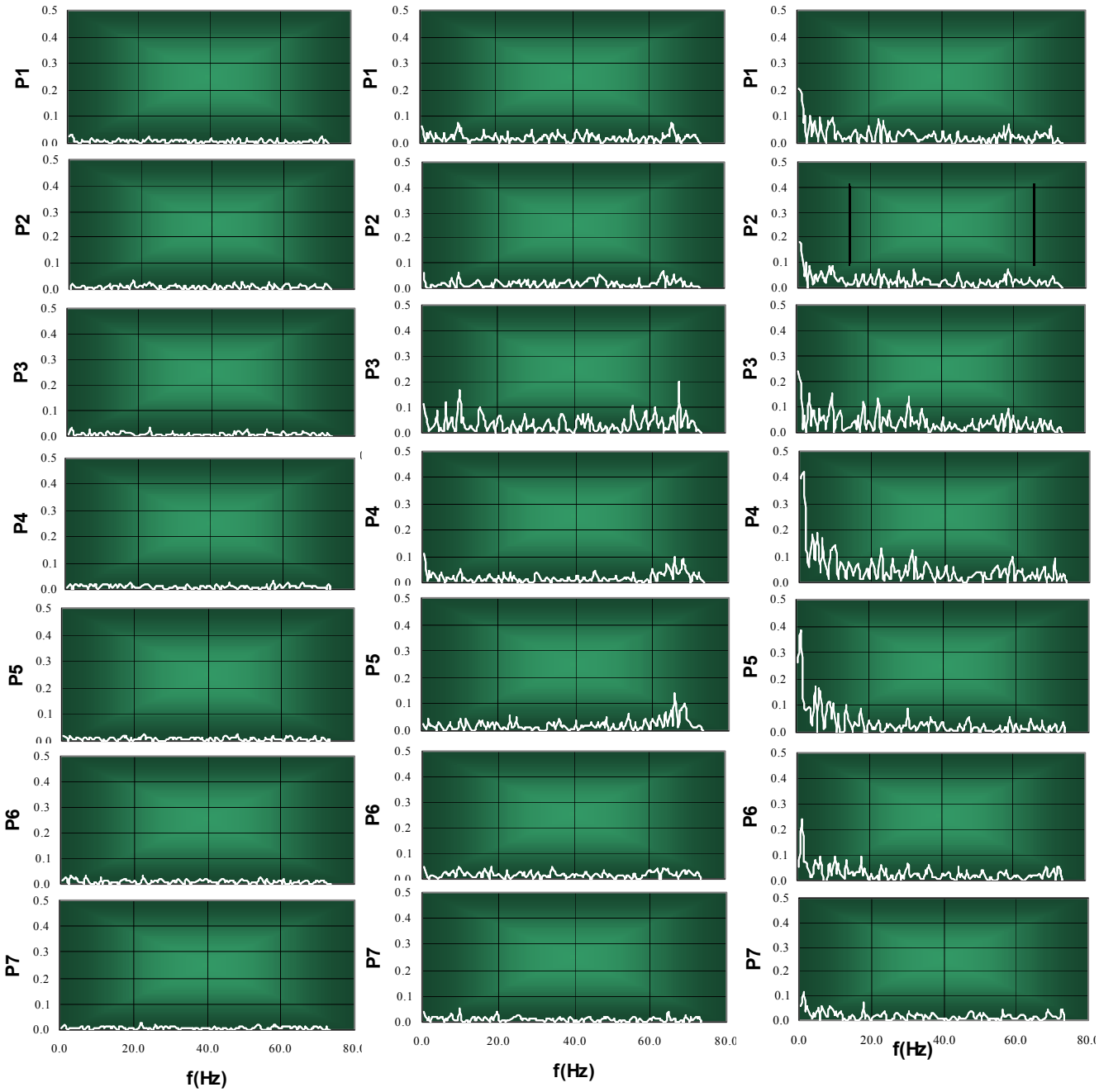

Fig. 9a α=1°　　Fig. 9b α=16°　　Fig. 9c α=25°

Fig. 9 Unsteady pressure spectra at different static angels of attack

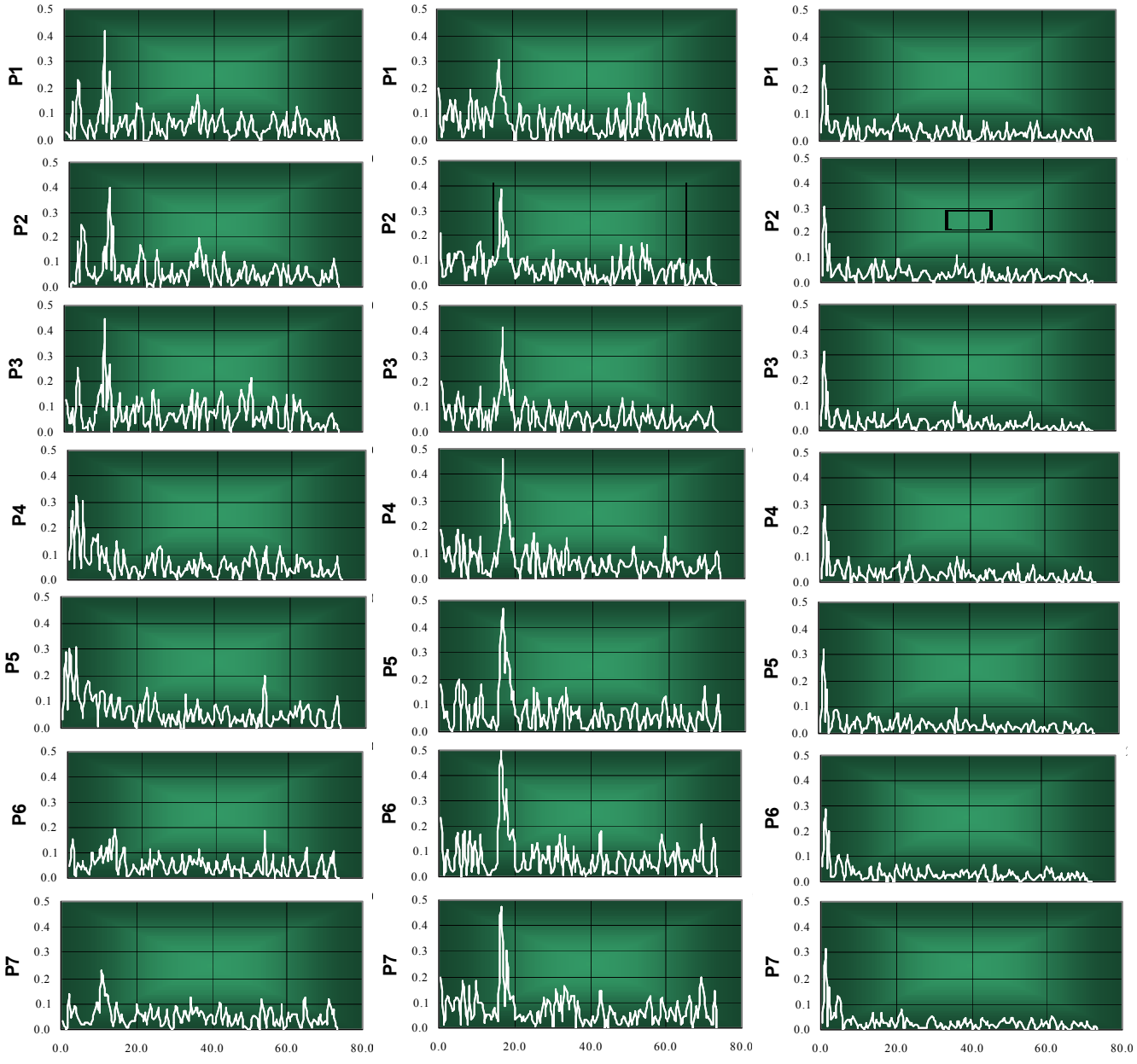

Fig. 9d α=29°

Fig. 9 e α=47°

Fig. 9 f α=51°

Fig. 9 Unsteady pressure spectra at different static angels of attack (cont.)

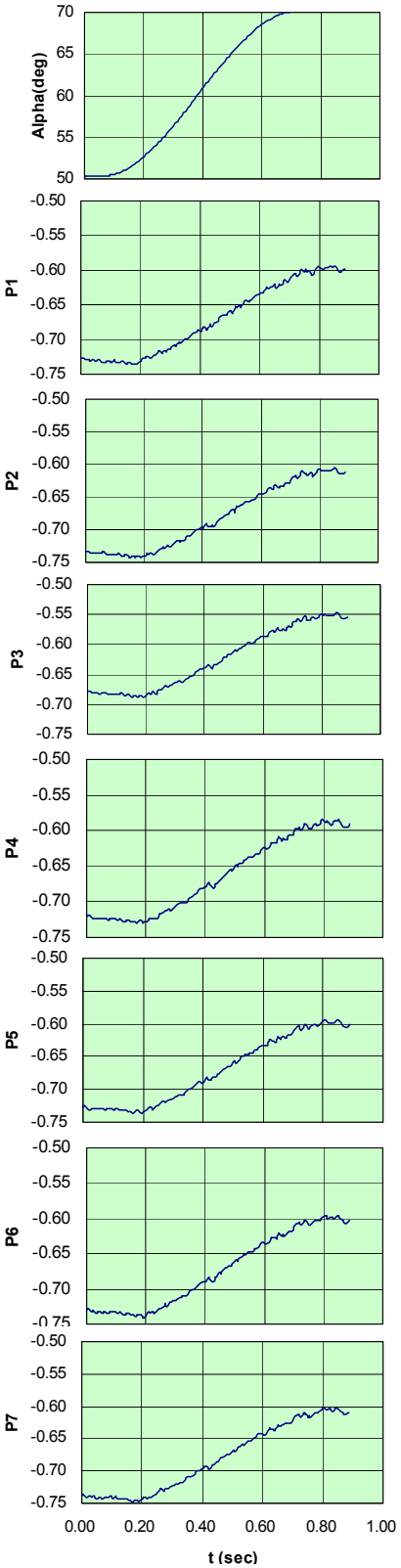

Fig. 10a pitch motion and pressures in time domain, α=50°→70°

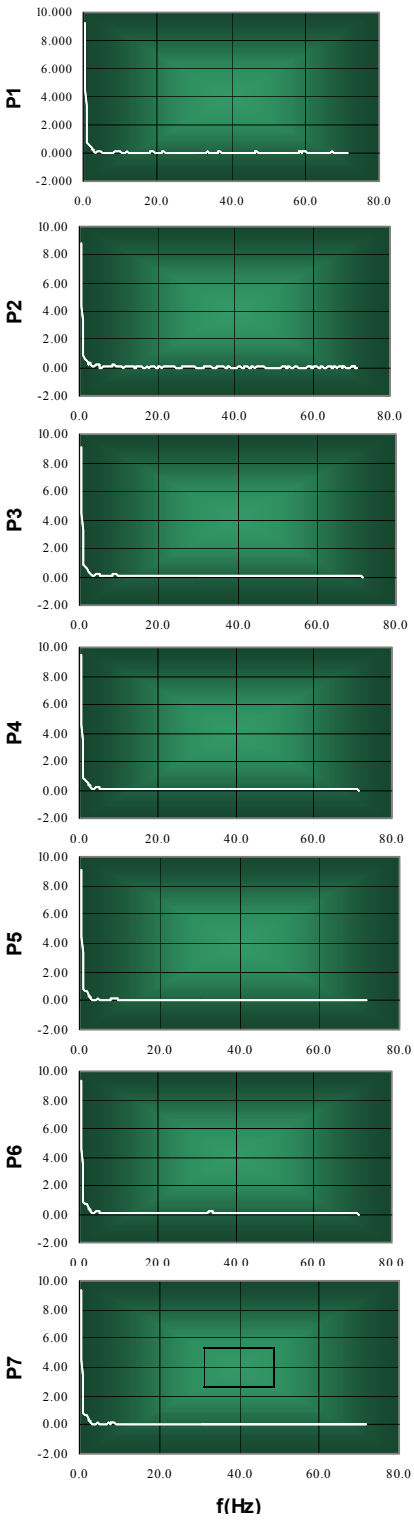

Fig. 10b pressure measurements in frequency domain, α=50°→70°

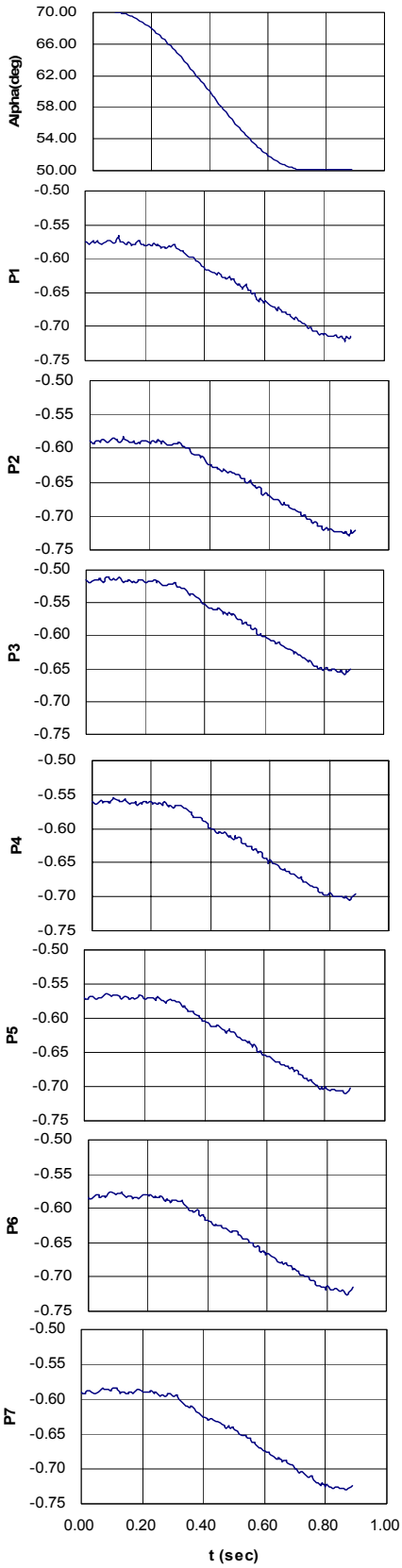

Fig. 11 pitch motion and pressures in time domain, α:70°→50°

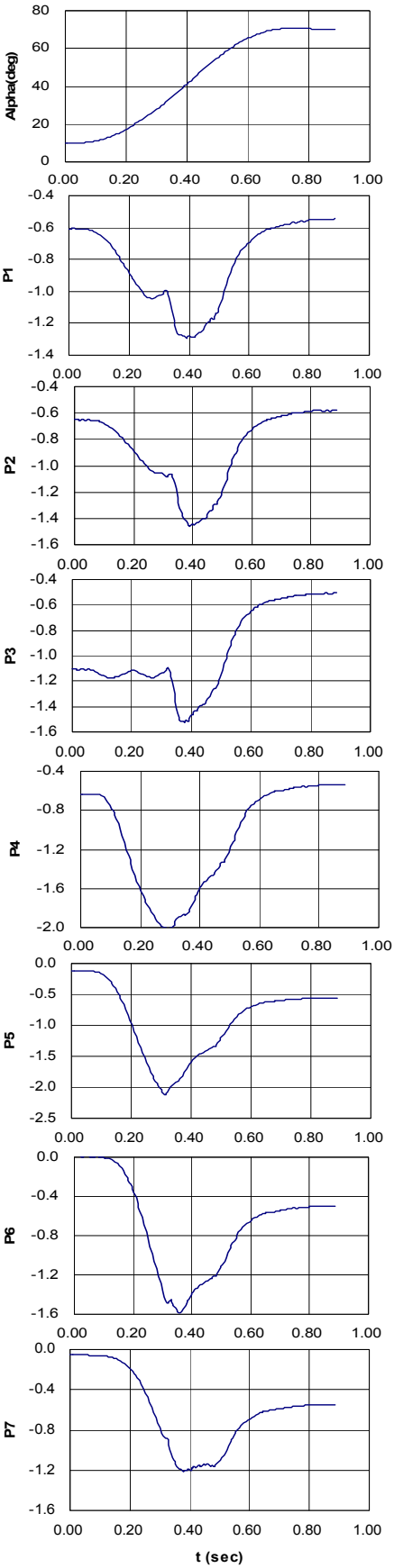

Fig. 12a pitch motion and pressures in time domain, α:10°→70°

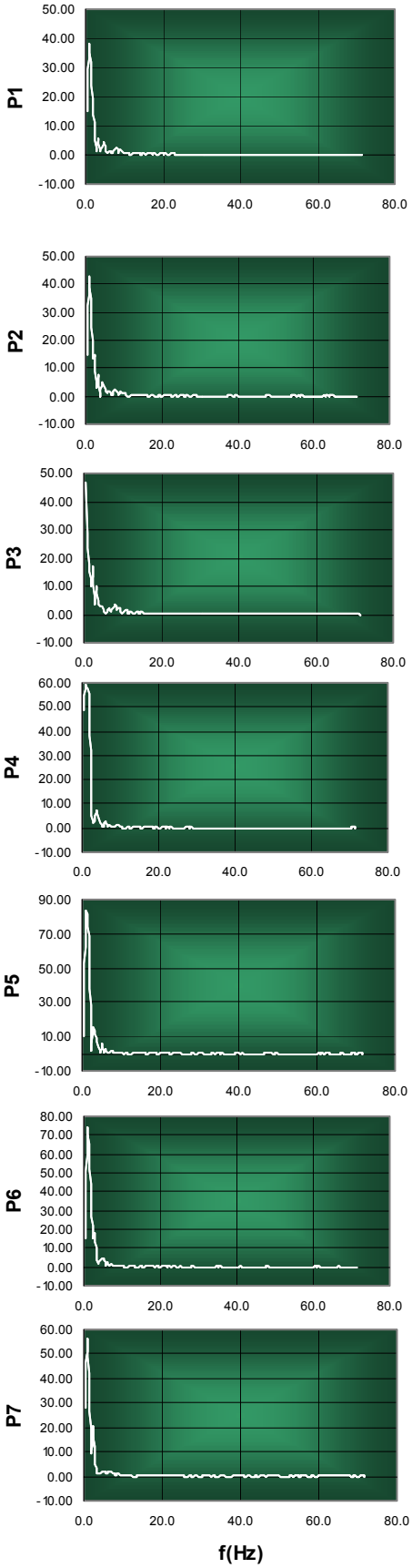

Fig. 12b pressures in frequency domain, α:10°→70°

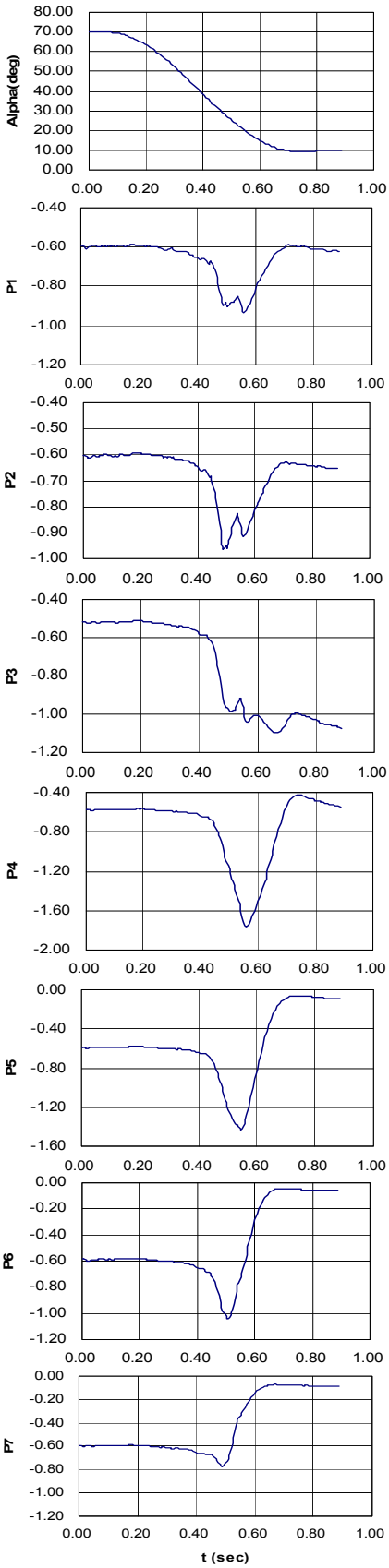

Fig. 13a pitch motion and pressures in time domain, α:70°→10°

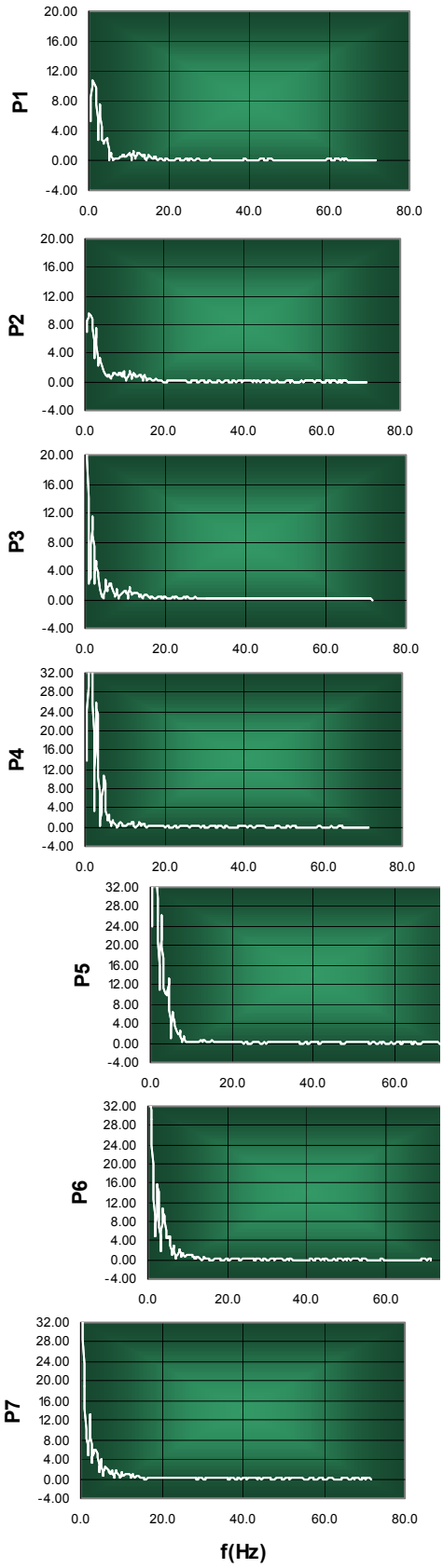

Fig. 13b pressures in frequency domain, α:70°→10°

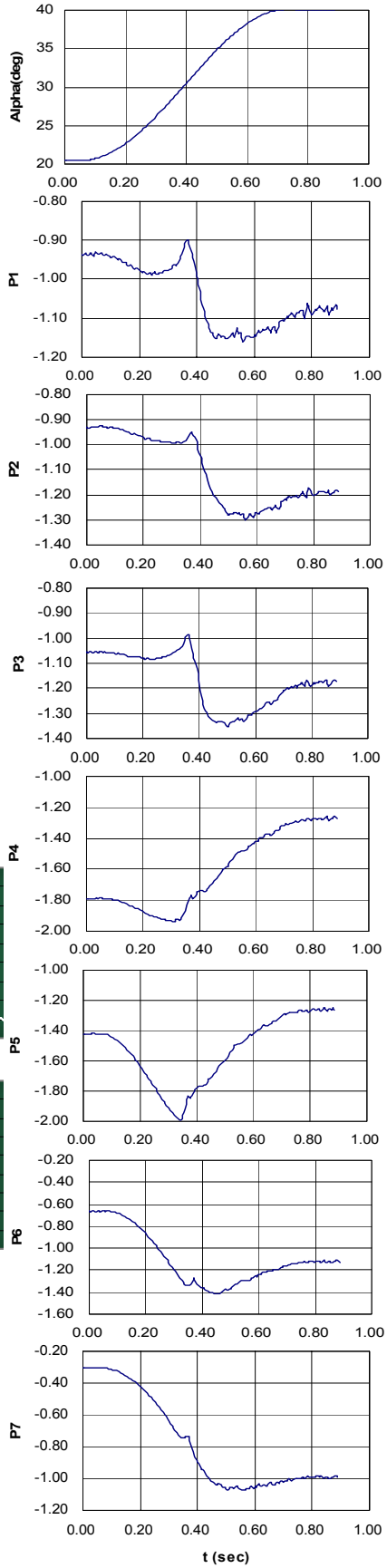

Fig. 14a pitch motion and pressure in time domain, α:20°→40°

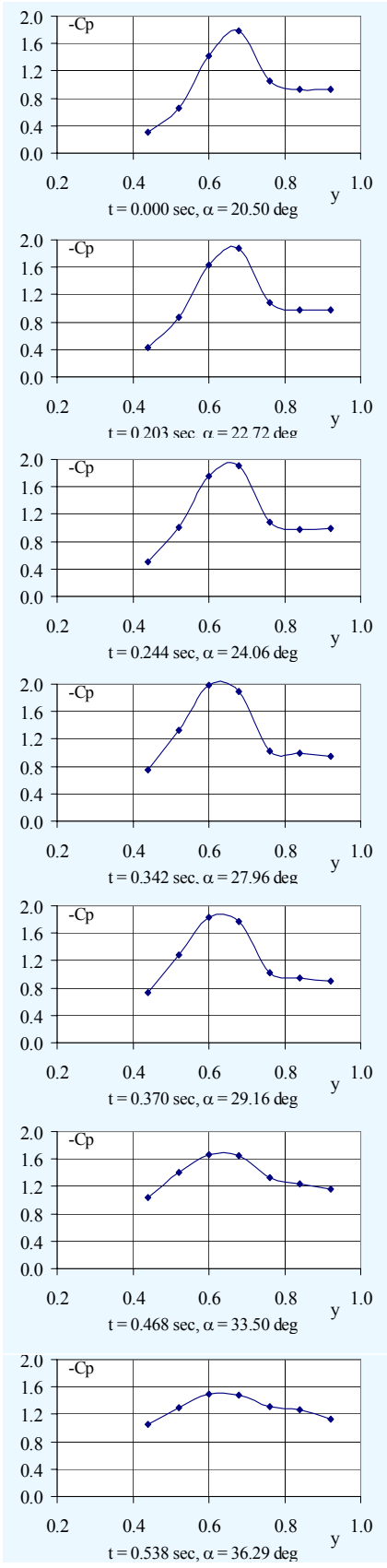

Fig. 14b pressures at instantaneous time, α:20°→40°

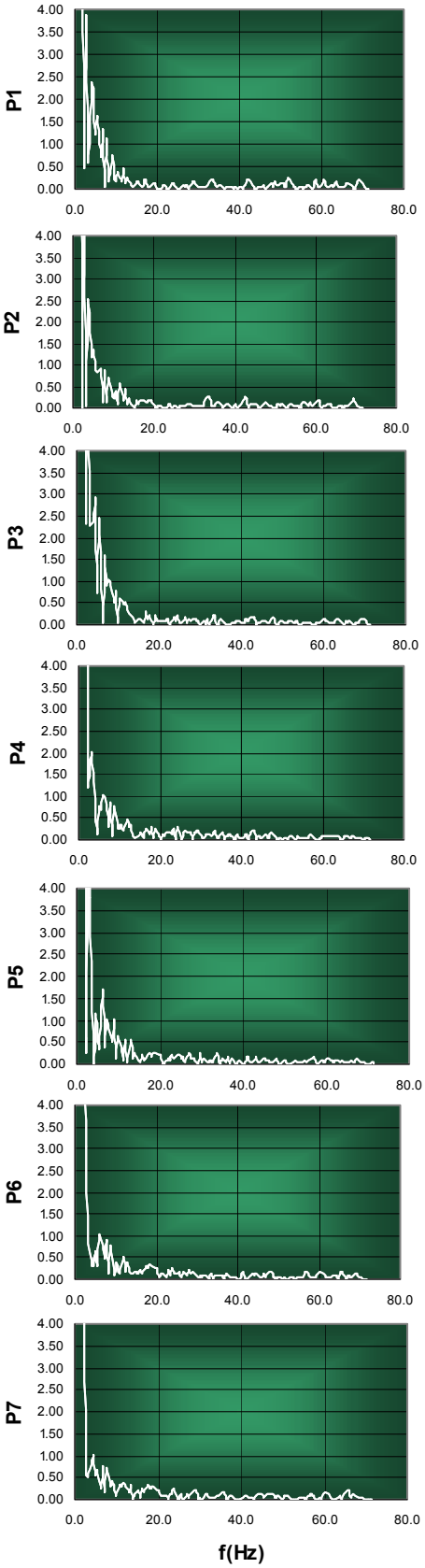

Fig. 14c pressures in frequency domain, α:20°→40°

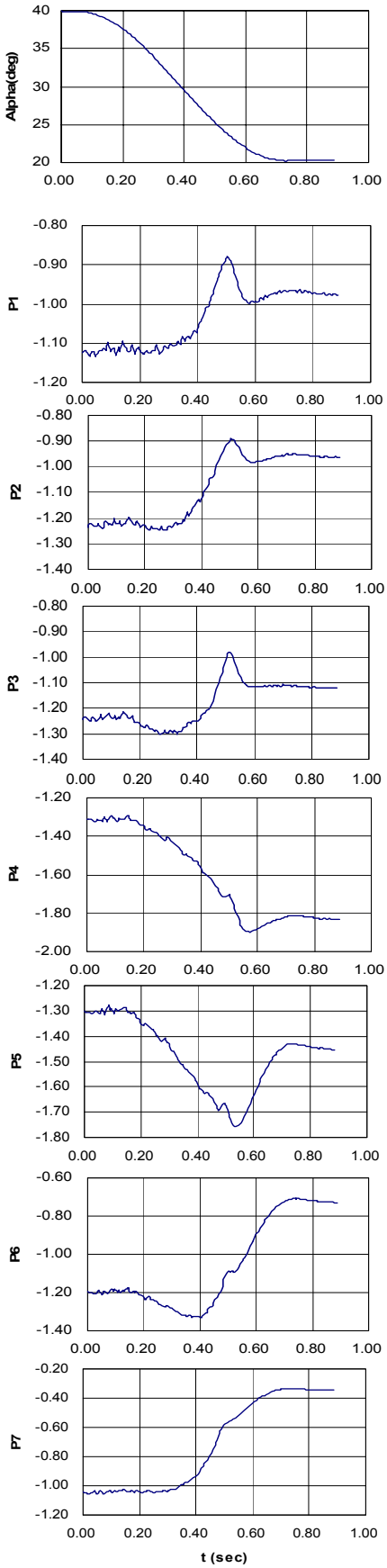

Fig. 15a motion and pressures in time domain, α:40°→20°

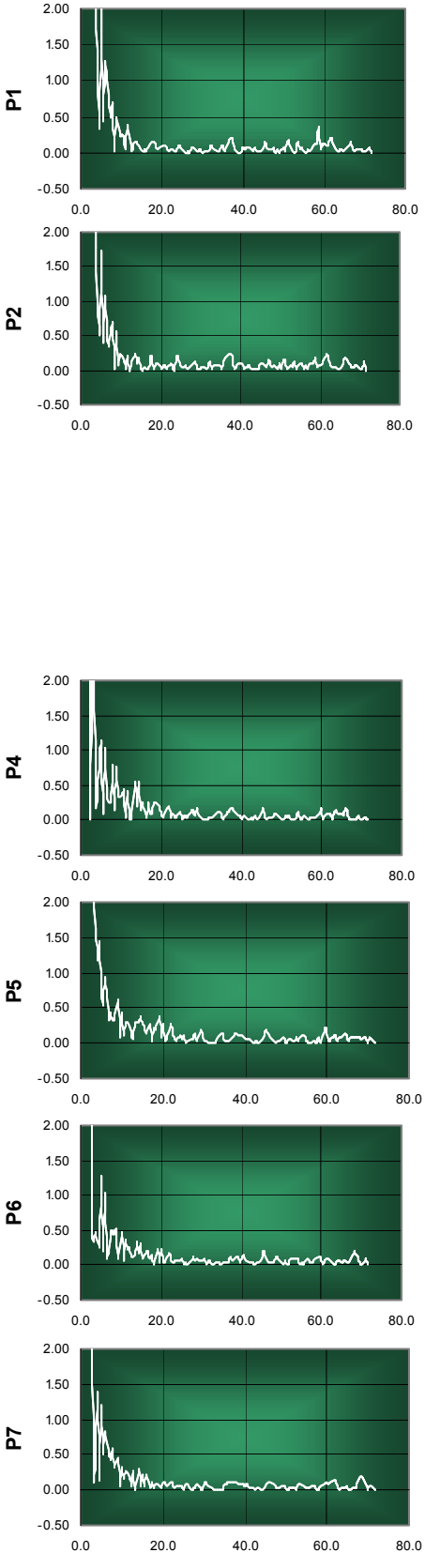

Fig. 15b pressures in frequency domain, α:40°→20°